









## Open Archive TOULOUSE Archive Ouverte (OATAO)

OATAO is an open access repository that collects the work of Toulouse researchers and makes it freely available over the web where possible.

This is an author-deposited version published in : <http://oatao.univ-toulouse.fr/>  
Eprints ID : 19801

**To link to this article** : DOI:10.1016/j.jeurceramsoc.2015.07.018  
URL : <http://dx.doi.org/10.1016/j.jeurceramsoc.2015.07.018>

**To cite this version** : Liu, Yinghui  and Vidal, Vanessa  and Roux, Sabine Le  and Blas, Fabien  and Ansart, Florence  and Lours, Philippe  *Influence of isothermal and cyclic oxidation on the apparent interfacial toughness in thermal barrier coating systems.* (2015) Journal of the European Ceramic Society, vol. 35 (n° 15). pp. 4269-4275. ISSN 0955-2219

Any correspondence concerning this service should be sent to the repository administrator: [staff-oatao@listes-diff.inp-toulouse.fr](mailto:staff-oatao@listes-diff.inp-toulouse.fr)

# Influence of isothermal and cyclic oxidation on the apparent interfacial toughness in thermal barrier coating systems

Y. Liu<sup>a,b</sup>, V. Vidal<sup>a,\*</sup>, S. Le Roux<sup>a</sup>, F. Blas<sup>a,b</sup>, F. Ansart<sup>b</sup>, P. Lours<sup>a</sup>

<sup>a</sup> Université de Toulouse; CNRS, Mines Albi, INSA, UPS, ISAE; ICA (Institut Clément Ader); Campus Jarlard, F-81013 Albi, France

<sup>b</sup> CIRIMAT, Centre Interuniversitaire de Recherche et d'Ingénierie des Matériaux, Université de Toulouse, UPS-INP-CNRS, Institut Carnot CIRIMAT, 118 Route de Narbonne, 31062 Toulouse, Cedex 09, France

## A B S T R A C T

In thermal barrier coatings (TBCs), the toughness relative to the interface lying either between the bond coat (BC) and the Thermal Grown Oxide (TGO) or between the TGO and the yttria stabilized zirconia topcoat (TP) is a critical parameter regarding TBCs durability. In this paper, the influence of aging conditions on the apparent interfacial toughness in Electron Beam-Physical Vapor Deposition (EB-PVD) TBCs is investigated using a specifically dedicated approach based on Interfacial Vickers Indentation (IVI), coupled with Scanning Electron Microscopy (SEM) observations to create interfacial cracks and measure the extent of crack propagation, respectively.

Keywords:  
TBC systems  
Oxidation  
Interfacial indentation  
EB-PVD  
Spallation  
Cracking

## 1. Introduction

Thermal barrier coatings (TBCs) are typically used in key industrial components operating at elevated temperature under severe conditions such as gas turbines or aero-engines, to effectively protect and isolate the superalloy metal parts, for instance turbine blades, against high temperature gases. Even though TBCs allow drastic improvement of component performance and efficiency [1,2], thermal strains and stresses resulting from transient thermal gradients developed during in-service exposure limit the durability of the multi-material system. TBCs exhibit complex structure and morphology consisting of three successive layers, deposited or formed on the superalloy substrate (Fig. 1), i.e. (i) the bond coat standing as a mechanical bond between the substrate and the topcoat; (ii) the Thermally Grown Oxide (TGO), an  $Al_2O_3$  scale that forms initially by pre-oxidation of the alumina-forming bond coat then slowly grows upon thermal exposure to protect the substrate from further high temperature oxidation and corrosion; (iii) The ceramic topcoat (TC), made of yttria-stabilized-zirconia (YSZ), the so-called thermal barrier coating itself whose role is mainly to insulate the superalloy substrate from high temperatures.

Electron Beam Physical Vapor Deposition (EB-PVD) and Air Plasma Spray (APS) are the two major coating processes implemented industrially for depositing YSZ. They generate different morphologies and microstructures and consequently different thermal and mechanical properties. The columnar structure, typical of the EB-PVD deposition, shows an optimal thermal-mechanical accommodation of cyclic stress resulting in high lateral strength. However, elongated (high aspect ratio) inter-columnar spaces roughly normal to the TBC, assist thermal flux conduction and penetration through the top-coat, which detrimentally increases the thermal conductivity of the system which can reach  $1.6\text{ W/m}\cdot\text{K}$ . APS TBCs are characterized by a lamellar structure, intrinsically much more efficient in terms of thermal insulation (conductivity as low as  $0.8\text{ W/m}\cdot\text{K}$ ) but less resistant to in-plane cyclic mechanical loading.

Regardless of the coating process, TBCs can suffer in-service damage as a consequence of the synergetic effect related to mechanical stress, high temperature and thermally activated growth of interfacial alumina. Failure can either occur cohesively within the top coat for APS TBCs or adhesively at interfaces between successive layers in EBPVD TBCs. Degradation of such systems usually occurs through the spallation of the topcoat resulting from severe delamination either at the BC/TGO or the TGO/TC interface. The resistance to spallation is intimately related to the capacity of interfaces of the complex TBC system to sustain crack initiation and propagation, which can be evaluated by measuring the interfacial

\* Corresponding author. Fax: +33 0 5 63 49 32 42.  
E-mail address: [Vanessa.Vidal@mines-albi.fr](mailto:Vanessa.Vidal@mines-albi.fr) (V. Vidal).

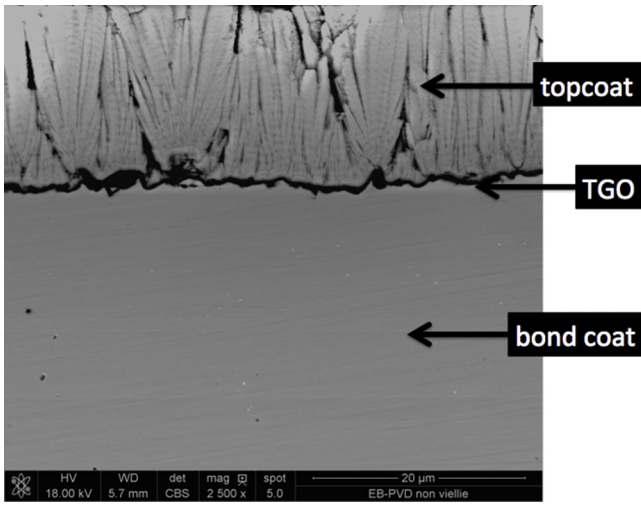


Fig. 1. SEM micrographs in cross-section of an EB-PVD TBC specimen.

toughness. Several methods have been proposed to achieve interfacial fracture toughness measurement for various substrate/coating systems, including “four point bending test” [3], “barb test” [4], “buckling test” [5], “micro-bending test” [6] and various indentation techniques [7–11]. This paper proposes to implement the Vickers hardness technique to estimate the interfacial toughness in EB-PVD TBCs as well as its evolution upon various isothermal and cyclic aging conditions. As a matter of fact, aging may provoke microstructural changes and residual stress development prone to enhance crack initiation and propagation. A tentative correlation between the conditions of aging, the induced microstructural changes and the concomitant evolution of toughness, necessary to understand and predict the durability of TBC systems, is detailed.

## 2. Materials and testing conditions

TBC systems processed by EB-PVD (150 μm thick), are provided by SNECMA-SAFRAN. Topcoats and bond-coats are industrial standards, respectively made of yttria stabilised zirconia (namely ZrO<sub>2</sub>-8 wt.% Y<sub>2</sub>O<sub>3</sub>) and β-(Ni,Pt)Al. Substrates are AM1 single crystal Ni-base superalloy disks, with a diameter of 25 mm and a thickness of 2 mm. All specimens are initially pre-oxidised to promote the growth of a thin protective Al<sub>2</sub>O<sub>3</sub> scale. Samples are cut, polished and subsequently aged using various oxidation conditions prior to interfacial indentation. In addition to the as-deposited condition, two series of results are analyzed separately. The first series is relative to isothermal oxidation, following 100 h exposure at 1050 °C, 1100 °C and 1150 °C respectively. As the exposure time is kept constant, the influence of the oxidation temperature can be specifically analysed. The second series, performed at a given temperature, (1100 °C) is dedicated to compare isothermal and cyclic oxidation behavior. Here again, the hot time at 1100 °C (i.e., 100 h), is the same for both tests. Fig. 1 shows the typical cross-sectional microstructure of an initial as-deposited EB-PVD TBC. Note that, after aging, a slight additional grinding is often required to prepare thoroughly the surface for interfacial indentation.

## 3. Interfacial indentation test

Various types of interfacial or surface indentation tests exist. They are performed either on the top surface of specimens, normal to the coating [12], or on cross-section, either within the substrate close to the interface [13] or at the interface between the substrate and the coating [9]. The latter, further developed in [14], employs a pyramidal Vickers indenter and can be applied for a large range of

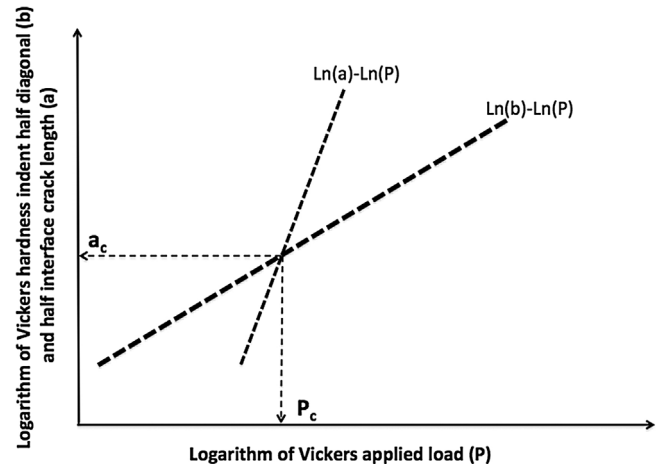


Fig. 2. Schematic representation of the intercept graphical method to determine the critical load required to generate interfacial crack [Ln(a) and Ln(b) are, respectively, plotted versus Ln(P)].

coating thicknesses (greater than ~100 μm). Typically, it is specifically used for investigating adhesion of TBC systems [7,8,14,15]. The principle of interfacial indentation is to accurately align one diagonal of the Vickers pyramid with the interface between the substrate and the coating while loading the system to hopefully generate the local delamination of the coating. In this case, resulting from the application of a high enough indentation force, an induced crack with roughly semi-circular shape instantaneously propagates. For a given aging condition, each indentation force  $P$  greater than a critical force  $P_c$  that must be estimated, generates a crack with radius  $a$  and an indent imprint with radius  $b$ .  $P_c$  and correlative the critical crack length  $a_c$  can not be determined using straightforward measurements but graphically correspond to the coordinates of the intercept between the apparent hardness line  $\text{Ln}(b)-\text{Ln}(P)$  showing the evolution of the imprint size versus the indentation force (master curve), and the  $\text{Ln}(a)-\text{Ln}(P)$  line giving the evolution of the crack size versus the indentation force (Fig. 2). The apparent interfacial toughness ( $K_{ca}$ ) is calculated as a function of the critical values according to the following relationship:

$$K_{ca} = 0.015 \frac{P_c}{a_c^{3/2}} \left( \frac{\left(\frac{E}{H}\right)_B^{1/2}}{1 + \left(\frac{H_B}{H_T}\right)^{1/2}} + \frac{\left(\frac{E}{H}\right)_T^{1/2}}{1 + \left(\frac{H_T}{H_B}\right)^{1/2}} \right) \quad (1)$$

where B and T stand, respectively, for the bondcoat and the topcoat.

In standard TBC systems, the thickness of the TGO is generally low, typically ranging from 0.7 μm (after initial pre-oxidation) to 7 μm (after long term exposure at high temperature), and is in any case much lower than the imprint of the indent resulting from the force range used for coating delamination purpose (Fig. 3). As a consequence, the influence of the TGO in terms of mechanistic issue is deliberately neglected [7]. However, it will be shown later that the thickness of the TGO has an influence on the location of the crack initiation and subsequently the propagation path.

## 4. Determination of Young's modulus and hardness

Young modulus  $E$  and hardness  $H$  strongly depend on the chemical composition and the process-induced microstructure of materials. In multi-materials such as TBCs, those mechanical characteristics change as composition changes throughout the entire thickness of the multi-layered system. If the nature of the single crystal substrate is essentially not affected by the overall deposition process, the morphology and microstructure of the top coat and to a lesser extent of the bond coat are strongly related to processing

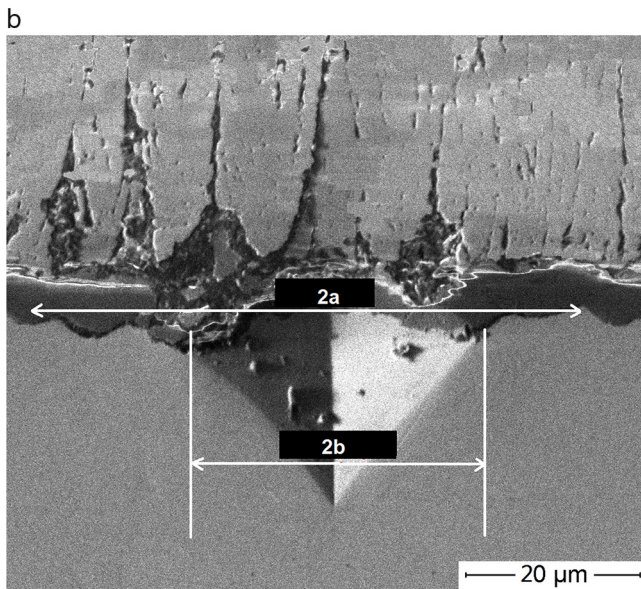
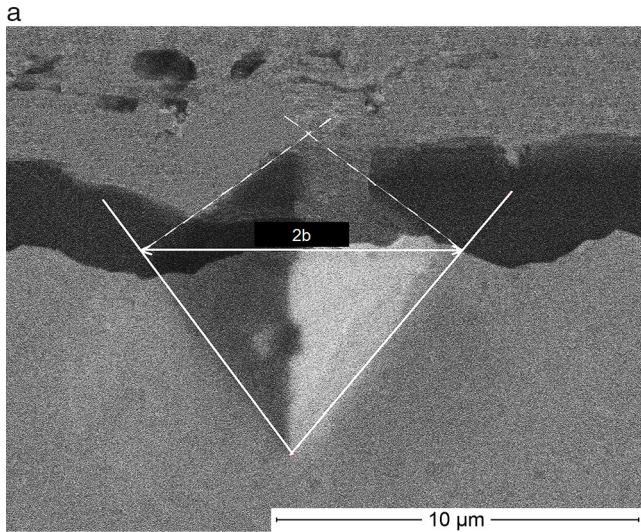


**Fig. 3.** SEM micrograph of indented samples oxidised 100 h at 1150 °C (a) indentation charge 0.981 N (corresponding to 100 g); (b) indentation charge 2943 N (corresponding to 300 g).

which in turn affects the mechanical properties. Strictly speaking, the mechanical response of the system to interfacial loading should depend on the elastic and plastic properties of all materials involved including that of the thermally grown oxide. However, a measurement of  $E$  and  $H$  of the growing oxide is not possible by means of standard micro and nano-indentation. The model detailed in [14] requires the knowledge of these characteristic parameters for the substrate and the coating. Accordingly, the TGO is assumed to play the role of a (three-dimensional) interface, thickening as temperature exposure increases and promoting, when loaded, spallation along the (two-dimensional) interface it shares with either the topcoat or the bond coat. Young modulus of the top coat  $E_T$  and hardness of both the bond coat  $H_B$  and the topcoat  $H_T$  are measured using the nano-indentation technique, implementing a Berkovich indenter. Details of the method can be found in [16]. Basically, considering the indentation force applied, hardness is evaluated by a simple and direct measurement of the indent imprint dimensions. Young's modulus is calculated by analyzing the purely elastic recovery of the plot relating the evolution of the applied force versus the in-depth displacement. For statistical reasons, hardness and Young modulus have been measured on 10 different locations within the

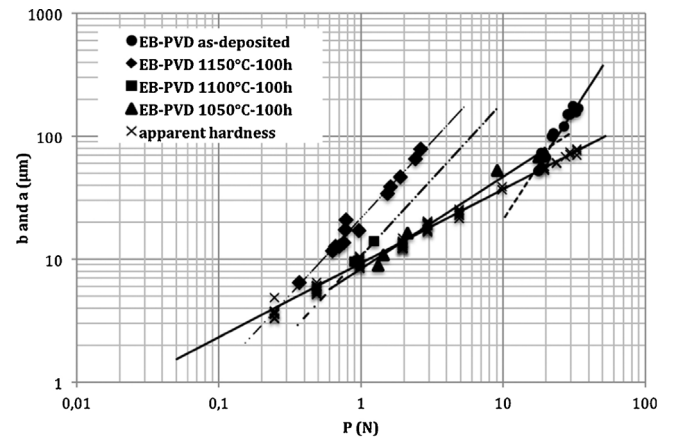


**Fig. 4.** Determination of critical loads to initiate interface cracking by Vickers indentation where  $a$  and  $b$  are plotted versus  $P$  using logarithmic scale.

bond coat and top coat respectively. Average values, experimentally determined, are given below:

- $E_B = 133$  GPa
- $E_T = 70$  GPa
- $H_B = 5.15$  GPa
- $H_T = 4.14$  GPa

## 5. Results and discussion

Typical examples of interfacial indentation results are given in Fig. 3. The indent imprint alone (Fig. 3a) or the indent imprint plus the induced crack (Fig. 3b) are shown for cases where the critical force to provoke crack formation is not reached or exceeded, respectively.

Fig. 4 gathers all data collected from experiments on as-deposited and isothermally oxidised TBCs. The linear relationship between  $\ln(P)$  and  $\ln(b)$ , plotting the so-called master curve of apparent hardness, with a slope close to 0.5 is in good agreement with the general standard formula relating the Vickers hardness (HV) of bulk materials to the ratio between the applied load  $P$  and the square of the indent diagonal length  $b^2$ . For a given oxidation temperature, the variation of the length  $a$  of the indentation-induced crack versus the applied load  $P$  also fits a single regression line on a Log-Log scale which can serve (as indicated in Section 3) to evaluate the critical load  $P_c$  necessary to initiate interfacial detachment. Note that for aged specimens, the critical force  $P_c$  (corresponding to the abscissa of the intercept between the master curve and  $\ln(P)$  vs  $\ln(a)$  plot) decreases as the oxidation temperature increases, thus indicating a thermally activated degradation of the interface. As a comparison, the as-deposited TBC can sustain much higher load prior to suffer interfacial debonding. Quantitatively, the critical force is respectively 0.3 N for 100 h oxidation at 1150 °C, 0.8 N for 100 h oxidation at 1100 °C, 2 N for 100 h oxidation at 1050 °C and about one order of magnitude higher (up to 16 N) for the as-deposited non oxidized TBC.

Using Eq. (1) and according to the values of  $E$  and  $H$  reported in Section 4, the apparent interfacial toughness is calculated and detailed in Fig. 5 for all investigated cases. Of course, correlatively to the thermally activated decrease of the critical force discussed above, toughness also decreases as the oxidation temperature increases. Besides, it was shown elsewhere [7] that for a given oxidation temperature, the interfacial degradation was similarly time-dependent too. This unambiguously shows that the propensity of the coating to detach from the substrate results from complex solid-state diffusion processes that impair the mechan-

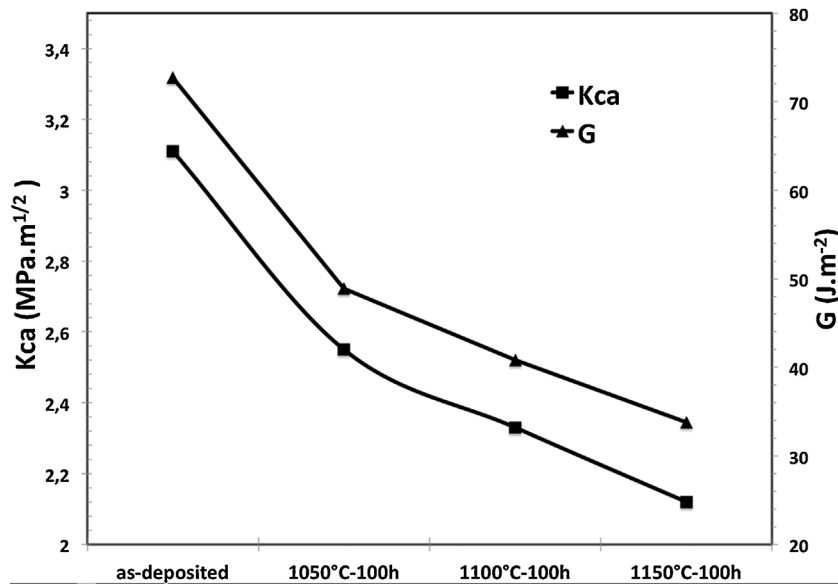


Fig. 5. Variation of interfacial toughness as a function of aging temperature.

ical strength of the interface through the formation of interfacial voids, local or extended rumpling or growth of oxide excrescences. As to compare to reference values taken from literature, the calculated interfacial toughness expressed in  $\text{MPa}\cdot\text{m}^{0.5}$  are converted into energy release rate  $G$  expressed in  $\text{J}\cdot\text{m}^{-2}$ . It comes that the as-deposited TBC exhibits a energy release rate  $G$  of  $72.7\text{J}\cdot\text{m}^{-2}$ , satisfactorily similar to that measured for EB-PVD TBCs by Eberl et al. ( $57.3 \pm 21.5\text{J}\cdot\text{m}^{-2}$ ) using a flexural test [6], and to a lesser extent by Snieszewski et al. ( $45\text{J}\cdot\text{m}^{-2}$ ) using interfacial indentation [17]. Generally speaking, values obtained from our experiments are consistent with results, reported in the literature, obtained using various experimental means including interfacial indentation, flexural test.

Beyond the mechanistic approach, the fractographic analysis gives interesting information on the mechanisms of crack initiation and further propagation, which can both vary depending on the aging conditions. Indeed, the enhancement of thermal activation as the oxidation temperature is raised results in the growth of a thicker alumina scale at the interface between the bond coat and the top coat. For as-deposited TBCs and TBCs aged at  $1050^\circ\text{C}$ , (i.e., for thin  $\text{Al}_2\text{O}_3$  oxide scales, respectively  $0.5\ \mu\text{m}$  and  $1.8\ \mu\text{m}$ ), cracks propagate preferentially along the interface between the TGO and the top coat. Conversely for TBC aged at  $1100^\circ\text{C}$  and  $1150^\circ\text{C}$ , with thick  $\text{Al}_2\text{O}_3$  oxide scales ( $3.4\ \mu\text{m}$  and  $5.3\ \mu\text{m}$ , respectively), cracks propagate predominantly along the TGO/bond coat interface.

This observation is consistent with results reported by Mumm et al. [18], using wedge imprint to generate delamination. It was shown that when the oxide thickness is lower than  $2.9\ \mu\text{m}$ , delamination extends predominantly within the TGO and TBC, whereas for thicknesses higher than  $2.9\ \mu\text{m}$ , degradation occurs along the interface between the bond coat and the TGO. Fig. 6 proposes a comprehensive map of cracking, which delimitates – within a graph plotting oxide thickness versus oxidation temperature – the two domains of initiation and propagation, either at the BC/TGO or the TGO/TC interfaces. These two domains consistently extend on either side of the critical thickness value proposed by Mumm et al. as the threshold for crack propagation at the TGO/bond coat interface. Note that the diagram includes oxide thicknesses measured for as-deposited, isothermally oxidized and cyclically oxidized (100 “1 h” cycles at  $1100^\circ\text{C}$ ) specimens. The oxide thickness was accurately estimated using image analysis on cross-sectional SEM micrographs showing the TGO layer, by dividing the total area of the

layer (expressed in  $\mu\text{m}^2$ ) by the developed length of its median axis (expressed in  $\mu\text{m}$ ). It was evaluated on thirty contiguous micrographs representing an equivalent length of  $4.8\ \text{mm}$  [19].

Mechanism of crack initiation and propagation is strongly related to the stress level and distribution within the multi-layer system. Apart from oxide growth stress (due to volume change during oxide growing), the main cause of mechanical strain and stress is the thermal expansion mismatch between layers of different thermal expansion coefficient during cooling and thermo-cycling. It is particularly critical upon cyclic oxidation as cumulative heating plus cooling is prone to dramatically enhance degradation. Under isothermal exposure, oxide growth stresses may be considered as the predominant contribution. According to Baleix et al. [20], the spallation at the metal/oxide interface system in a  $\text{Cr}_2\text{O}_3$  forming heat resistant cast steels, occurs through the so-called oxide buckling for scale thickness equal or higher than  $4\ \mu\text{m}$ . In the frame of the strain-energy model for spallation, it is shown in this case that the interfacial fracture energy for buckling decreases from  $5\text{J}\cdot\text{m}^{-2}$  to  $2\text{J}\cdot\text{m}^{-2}$  as the oxide thickens from  $7\ \mu\text{m}$  to  $9\ \mu\text{m}$ . This suggests a progressive degradation of the interface as the oxidation mechanisms are enhanced through an extended exposure time.

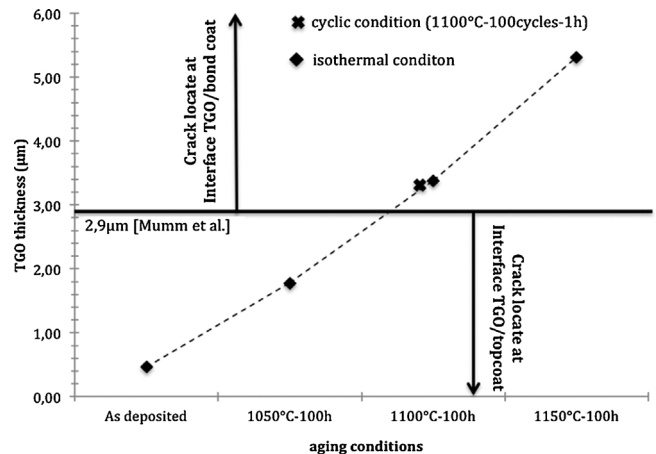
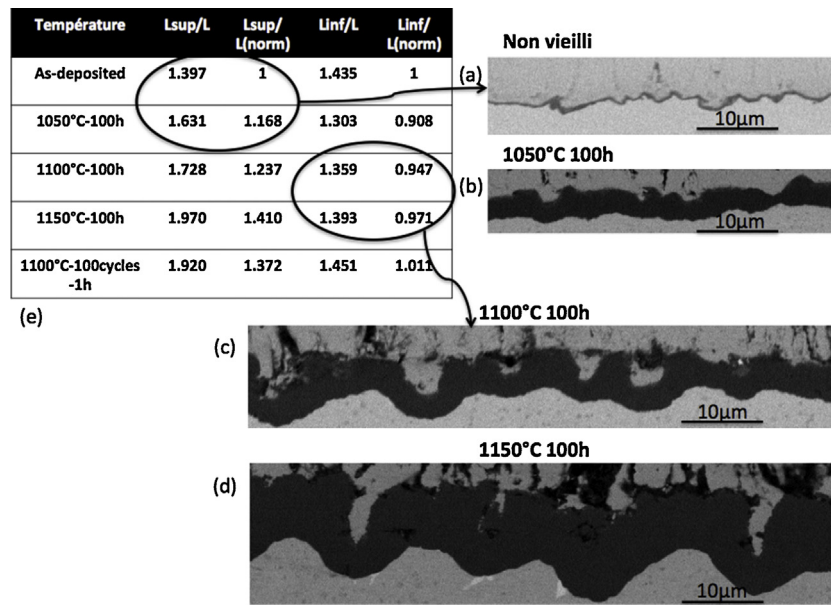


Fig. 6. Map of cracking as a function of oxidation conditions based on oxide thickness criterion.  $\blacklozenge$  and  $\times$  dots correspond to TGO thickness for isothermal (100 h) and cyclic ( $1100^\circ\text{C}$ -100 cycles-1 h) oxidation, respectively.



**Fig. 7.** Cross-sectional SEM micrographs of specimens (a) as deposited, (b) aged 100 h at 1050 °C, (c) aged 100 h at 1100 °C, (d) aged 100 h at 1150 °C, (e) variation of interfacial folding index as a function of aging conditions. Note that cracks locate preferentially at the TGO-topcoat interface for as-deposited specimen and specimens aged at 1050 °C (relevant parameter L<sub>sup</sub>/L) and at the bon coat/TGO interface for specimens aged at 1100 °C and 1150 °C (relevant parameter L<sub>inf</sub>/L).

Formally, buckling of oxide prior to detachment for the onset to spallation is very comparable to the generation of cracks at the interface between the bond coat and the TGO promoted by indentation in TBCs systems. Indeed, depending on the oxide thickness and the strength of the metal oxide interface, two different routes for spallation are generally reported. In the case of a strong interface for thin oxides, i.e., a high toughness or high fracture energy, compressive shear cracking develops in the oxide. Consequently, detachment of oxide particles occurs by wedge cracking. In the case of a weak interface for thicker oxides, i.e., low toughness or fracture energy, the oxide may detach from the metal in the form of buckles. Evans et al. [21] showed elsewhere that the energy stored within the TGO increases as the TGO thickens, and contributes only to the delamination at the TGO/bond coat interface. As a consequence, the fracture energy or toughness of the interface TGO/bond coat may decrease as the oxidation proceeds and the oxide thickens. Beyond a given oxide thickness threshold, namely around 3 μm for 150 μm thick EB-PVD TBCs, the toughness of the TGO/bond coat interface becomes lower than that, essentially unchanged, of the TGO/topcoat interface, yielding to a change in delamination location.

In addition, as indicated in Fig. 2, the slopes of the various lines plotted for various conditions of aging in order to determine the critical force to initiate interfacial cracking are different. This clearly indicates that whatever the critical force is, the possibility to extend a crack requires more or less mechanical energy depending on the configuration, i.e., the specific morphology of the interface. To address this, a straightforward image analysis methodology detailed in [19] is applied on SEM cross-sectional micrographs to determine the roughness of the internal interfaces, between the bond coat and the TGO, and the TGO and the top coat (Fig. 7).

According to this approach, a rumpling or folding index is defined as the ratio between the developed length of the interface and the horizontal projected length measured on 30 contiguous micrographs corresponding to an equivalent length of 4.8 mm. This index is a relevant indicator of the tortuosity of the interfaces. Fig. 7 gives values for both the TGO-top coat interface (upper profile), the bond coat – TGO interface (lower profile) as well as normalised values (obtained by dividing the values by the reference one (as-

deposited TBC)). Both isothermal aging (100 h at 1150 °C, 1100 °C and 1050 °C) and cyclic aging (100 cycles of 1 h at 1100 °C) are investigated. Cross-sectional SEM micrographs illustrating the evolution of the thickness and morphology of the TGO for various isothermal oxidation temperatures are also shown in Fig. 7. Note that the interfacial corrugation of the as-deposited TBC is significant, both for the upper and lower profiles, which accounts directly for the roughness of the initial substrate. However, the upper profile is slightly smoother than the lower profile, suggesting a leveling effect of the initial oxidation intrinsic to the EB-PVD deposition process. In all cases, aging results in an enhancement of the upper profile tortuosity: the higher the oxidation temperature, the more pronounced the associated folding effect. The evolution of the lower profile is more complex to analyze. Indeed, aging at 1050 °C leads to a significant decrease (about 10%) with respect to the initial value of the as-deposited TBC. The interface between the oxide and the bond coat becomes smoother as oxidation progresses, indicating a total absence of interfacial folding. This observation is not consistent with results presented in [22] reporting the occurrence of rumpling even under isothermal oxidation. For aging at 1100 °C and 1150 °C, L<sub>inf</sub>/L – though remaining lower than the reference value – is higher than at 1050 °C. Note that for cyclic oxidation at 1100 °C, the tortuosity of the bond coat/TGO interface is slightly greater than that of the reference, as-deposited TBC and of the TBC aged at the same temperature over the same hot time upon isothermal oxidation (Fig. 7). Globally speaking, the normalised folding index indicating the propensity of the multi-materials system to rumpling remains lower than 1 for the interface between the bond coat and the TGO. This clearly indicates that oxidation over short term exposure, either isothermal or cyclic, does not provoke any corrugation of the interface. In contrast, the interface between the TGO and the top coat tends to undulate as it is exposed to high temperature either upon isothermal or cyclic conditions. It is however unusual to evaluate rumpling considering the interface between the TGO and the top coat. It is much more common to monitor the evolution of the bond coat/TGO interface. It can be assumed that (i) rumpling is negligible, or at least little pronounced, under isothermal oxidation, (ii) thermal aging under 100 cycles – though prone to generate more degradation than isothermal exposure – is

not sufficient to provoke significant rumpling. Though equivalent in terms of hot-time, cyclic oxidation (1 h-cycle) does not degrade further the interfacial toughness nor the tortuosity of the interface which, taking into account the assumed severity, highly constraining effect of the cooling phases of cycles, is probably due to the low number of cycles imposed to the TBC.

Folding effects and subsequent cracks propagation routes can be related to the evolution of oxide thickness. Indeed, for thin oxides, typically with thickness lower than 2.9  $\mu\text{m}$ , for the as-deposited and 1050 °C oxidised TBC, indentation-induced cracks initiate and further propagate at the TGO – top coat (outer) interface which exhibits in both cases apparent toughness higher than 3  $\text{MPa}\cdot\text{m}^{0.5}$ . This suggests a high adherence of the TGO in good agreement with previous results commonly reported in the literature. Between the reference, as-deposited TBC and the TBC oxidised at 1050 °C, a huge difference in the folding index is however noted. It is almost 20% higher in the second case as a consequence of a significant roughening of the interface upon oxidation. Though the location of crack initiation and propagation is the same for the two conditions; the evolution of the indentation force versus the size of crack produced is highly specific of each case as it is directly relative to the tortuosity of the interface. Indeed the increase in force is much less pronounced for the smoothest interface corresponding to the case of the as-deposited non-aged TBC and reciprocally.

For oxides thicker than 2.9  $\mu\text{m}$ , in the case of TBC oxidised at 1100 °C and 1150 °C, indentation-induced cracks propagate at the bond coat/TGO (inner) interface. For the two cases, the apparent toughness of the involved interface is lower than 2.6  $\text{MPa}\cdot\text{m}^{0.5}$ . While thickening, the alumina scale progressively loses adhesion from the bond coat, which transfers the location of crack initiation and propagation accordingly to commonly admitted models for spallation. The folding index of this inner interface is similar in both cases and very close to that of the outer interface of the as-deposited TBC. This results in a similar tortuosity of the interfaces (either inner or outer), where cracks form and extend and accounts for the similar evolution of the “required force” versus “size of crack produced” plots, experimentally established.

While thickening, the thermally grown oxide develops non uniformly as clearly shown on micrographs in Fig. 7. Preferential growth of oxide can occur in zones, typically within intercolumnar spaces of the EB-PVD TBC, where the oxidation kinetics is faster as more room is available for oxide to develop. The interface profile generated by this inhomogeneous growth shows local excrescences, clearly visible in Fig. 7c. The occurrence of such protrusions, whose formation is thermally activated can have various consequences – with opposite effects – on the mechanical strength of the interface. Indeed, an increase in interface tortuosity may contribute to a loss of adhesion as the result of local mechanical stresses and stress concentration responsible for enhanced crack initiation. Once initiated and to further degrade the system, cracks have to propagate. However, it is assumed that the presence of local excrescences acting as mechanical pegs can limit the propagation, thus preventing from early spallation.

## 6. Conclusion

The adhesion and counterpart spallation of EB-PVD TBC systems is investigated using various approaches including isothermal and cyclic oxidation at various temperatures and interfacial indentation of both as-deposited and oxidized systems. This former characterization is dedicated to evaluate the apparent toughness shown by the interface between the inner bond coat ( $\beta$ -NiPtAl) and the outer top coat (Yttria-Stabilised Zirconia) before and after thermal aging or cycling. For the as-deposited TBC, only short-term pre-oxidized to promote the formation of a dense, slowly growing alumina

scale acting as diffusion barrier, the interfacial TGO is rather thin (less than 0.5  $\mu\text{m}$ ). Upon aging, the TGO layer grows according to a roughly parabolic kinetics. In all cases, two distinct interfaces formed between the bond coat and the TGO (inner interface), and the TGO and the top coat (outer interface), respectively, must be considered. Driven by the growth of the TGO layer, both interfaces undergo morphological and roughness changes as the TGO thickens. The tortuosity of the interfaces, observed by SEM in cross-sections, is quantified by a folding or rumpling index estimated using image analysis. It is shown that both the oxide thickness and the folding index of the inner and outer interfaces, have a strong impact on the localization of the indentation-induced crack initiation, the path for propagation of crack once initiated and the ease or difficulty for crack to propagate. The apparent toughness deduced from interfacial indentation decreases as the 100-h isothermal-oxidation temperature increases from 1050 °C to 1150 °C indicating a progressive, thermally activated propensity for the degradation of TBC systems, as obviously expected. Apparent interfacial toughness controlled by interfacial roughness, TGO thickness and mostly by the temperature and time of isothermal or cyclic oxidation is a key parameter to address the mechanics and mechanisms of crack initiation and propagation prior to detrimental spallation of TBC systems. This is of course not the sole parameter entering in the implementation of possible models to predict TBC lifetime. Further improving the understanding of TBC behavior under severe oxidation exposure would require considering the fine variations of microstructural details and the evolution of the stored elastic strain energy, within each individual layer (Ni base single crystal,  $\beta$ -NiPtAl bond coat,  $\text{Al}_2\text{O}_3$  TGO and Yttria-Stabilised-Zirconia) and from one constitutive layer to another, as well as the substrate geometry to get closer to real in-service conditions.

## References

- [1] N. Padture, M. Gell, E.H. Jordan, Thermal barrier coatings for gas-turbine engine applications, *Science* 296 (2002) 280–284.
- [2] B. Goswami, K. Ray Ashok, S.K. Sahay, Thermal barrier coating system for gas turbine application—a review, *High Temp. Mater. Processes* 23 (2004) 73–92.
- [3] P. Thery, M. Poulain, M. Dupeux, M. Braccini, Adhesion energy of a YPSZ EB-PVD layer in two thermal barrier coating systems, *Surf. Coat. Technol.* 202 (2007) S648–S652.
- [4] S. Guo, Y. Tanaka, and Y. Kagawa, Effet of interface roughness and coating thickness on interfacial shear mechanical properties of EB-PVD Yttria-Partially Stabilized Zirconia thermal barrier coating systems, *J. Eur. Ceram. Soc.* 27 (2007) S3425–31.
- [5] S. Faulhaber, C. Mercer, M. Moon, J. Hutchinson, A. Evans, Buckling delamination in compressed multilayers on curved substrates with accompanying ridge cracks, *J. Mech. Phys. Solids* 54 (2006) S1004–S1028.
- [6] C. Eberl, X. Wang, D.S. Gianola, T.D. Nguyen, M.Y. He, A.G. Evans, K.J. Hemker, In Situ Measurement of the toughness of the interface between a thermal barrier coating and a Ni alloy, *J. Am. Ceram. Soc.* 94 (Suppl. 1) (2011) 120–127.
- [7] J. Sniezewski, V. Vidal, P. Lours, Y. Le Maout, Thermal barrier coatings adherence and spallation: interfacial indentation resistance and cyclic oxidation behaviour under thermal gradient, *Surf. Coatings Technol.* 204 (2009) 807–811.
- [8] J. Lesage, M.H. Staia, D. Chicot, C. Godoy, P.E.V. De Miranda, Effect of thermal treatments on adhesive properties of a NiCr thermal sprayed coating, *Thin Solid Films* vol. 377–378 (2000) 681–686.
- [9] D. Choulier, Contribution à l'étude de l'adhérence de revêtements projetés à la torche à plasma. Modélisation et utilisation d'un test d'indentation à l'interface », in: Thèse de doctorat, Université de Technologie, Compiègne, 1989.
- [10] J.L. Vasinonta, A. Beuth, Measurement of interfacial toughness in thermal barrier coating systems by indentation, *Eng. Fracture Mech.* 68 (2001) S843–S860.
- [11] W.G. Mao, J. Wan, C.Y. Dai, J. Ding, Y. Zhang, Y.C. Zhou, C. Lu, Evaluation of microhardness, fracture toughness and residual stress in a thermal barrier coating system: a modified Vickers indentation technique, *Surf. Coat. Technol.* 206 (2012) 4455–4461.
- [12] J.B. Davis, H.C. Cao, G. Bao, A.G. Evans, The fracture energy of interfaces: an elastic indentation technique, *Acta Metall. Mater.* 39 (5) (1991) 1019.
- [13] J. Colombon, B. Capelle, Contraintes Résiduelles et Nouvelles Technologies, *Recueil de Conférences, CETIM*, 1990, p. 99.

- [14] D. Chicot, P. Démarécaux, J. Lesage, Apparent interface toughness of substrate and coating couples from indentation tests, *Thin Solid Films* 283 (1996) 151–157.
- [15] L.T. Wu, R.T. Wu, X. Zhao, P. Xiao, Microstructure parameters affecting interfacial adhesion of thermal barrier coatings by the EB-PVD method, *Mater. Sci. Eng. A* 594 (2014) 193–202.
- [16] B.K. Jang, H. Matsubara, Hardness and Young's modulus of nanoporous EB-PVD YSZ coatings by nanoindentation, *J. Alloys Compd.* 402 (2005) 237–241.
- [17] Julien SNEZEWSKI, Etude in situ sous gradient thermique de l'écaillage d'alliages allumino-formeurs et de barrières thermiques aéronautiques, Thèse de doctorat en Génie Mécanique, Mécanique des Matériaux, under the supervision of Philippe Lours and Yannick Le Maout, Mines Albi, Université de Toulouse 2008.
- [18] D.R. Mumm, A.G. Evans, On the role of imperfections in the failure of a thermal barrier coating made by electron beam deposition, *Acta Mater.* 48 (2000) 1815–1827.
- [19] S. Le Roux, F. Deschaux-Beaume, T. Cutard, P. Lours, Quantitative assessment of the interfacial roughness in multi-layered materials using image analysis: application to oxidation in ceramic-based materials, *J. Eur. Ceram. Soc.* 35 (2015) 1063–1079.
- [20] S. Baleix, G. Bernhart, P. Lours, Oxidation and oxide spallation of heat resistant cast steels for superplastic forming dies, *Mater. Sci. Eng. A* 327 (2002) 155–166.
- [21] A.G. Evans, D.R. Clarke, C.G. Levi, The influence of oxides on the performance of advanced gas turbines, *J. Eur. Ceram. Soc.* 28 (2008) 1405–1419.
- [22] V.K. Tolpygo, D.R. Clarke, On the rumpling mechanism in nickel-aluminide coatings part II: characterization of surface undulations and bond coat swelling, *Acta Mater.* 52 (2004) 5129–5141.